Supplementary Information

Porphyrinic N_4 channels of zinc ions for electrochemical reversibility of zinc plating/stripping

Hyun-Woo Kim [a,§], *Eunyoung Cho* [a,§], *Myung-Jun Kwak* [b], *Jeongin Lee* [a], *Hosik Lee* [a],

*Chihyun Hwang** [b], *and Hyun-Kon Song** [a]

[a] School of Energy and Chemical Engineering, UNIST, Ulsan 44919, Korea.

[b] Advanced Batteries Research Center, Korea Electronics Technology Institute (KETI), Seongnam, Gyeonggi 13509, Korea.

Keywords: zinc-ion battery, reversibility, ion channel, porphyrin, metalation

Video clips for samples

Video S1, S2. Bubble generation from bare zinc metal surface

Experimental

Anodes. 1mL of ethanolic solution of 0.1 mM H_2PP-4COO (PorphyChem) was dropped on zinc foil (16 mm diameter, 99.98%, Alfa Aesar). The porphyrinic solution was allowed to be on the substrate for 1 min. After being rinsed with ethanol, the zinc foil was dried in oven at 80 ^oC for 4 h (H_2PP-4COO αSEI layer or **1**). The surface of the sample was found to be yellow-colored after drying. The zinc foil with H_2PP-4COO αSEI layer was immersed in 0.7 M zinc acetate solution for 60 min, rinsed with water and then heated under vacuum at 180 ^oC for 8 h ([Zn]PP-4COO-(Zn) αSEI layer or **2**).

Cathodes. 25 mg cm^{-2} MnO_2 (Alfa Aesar) with polytetrafluoroethylene (PTFE) and carbon black (CB) (MnO2 : PTFE : CB = 75: 20: 5 in mass) was loaded on 10 um-thick titanium foil by a roll-to-roll processing. ZIB pouch cells were fabricated with sandwiching a glass fiber separator by the MnO_2 cathode and a zinc foil. The aqueous electrolyte contained 2 M $ZnSO_4$ and 0.5 M $MnSO_4$. ZVO nanobelt was synthesized as another cathode active material to investigate the HER-suppressing capability of **2**. 2 mmol vanadium (V) oxide was dissolved in 21 ml distilled water for 1 h. 5 ml hydrogen peroxide was introduced dropwise to the solution at 40 ^oC. The mixture was stirred at 500 rpm for 30 min. 0.5 mmol zinc acetate was introduced to the mixture for 30 min while stirring at 500 rpm. The solution placed in a Teflon-lined autoclave was heated by 2 ^oC min^{-1} to 210 ^oC for 48 h. Solid material was recovered from the solution by filtration and then freeze-dried at -80 ^oC.

Characterization. SEM (Hitachi SU7000 FE-SEM) and TEM (JEOL JEM-2100F) for morphological and elemental investigation. XRD (Rigaku D/MAX2500V/PC) with Al Kα

irritation source at 600W (ThermoFisher K-alpha spectrometer) for identifying long-range ordering.

Electrochemical measurements. Beaker cells for three-electrode configuration with Ag/AgCl as the reference electrode. 2032-coin cells with a glass fiber separator (Whatman GF/C) between two electrodes. Zinc metal foil, used after mechanical polishing. 2 M $ZnSO_4$ (aq) as the electrolyte. Galvanostatic battery cell tests by a cycle tester (Wonatech WBCS3000). EIS (VMP3 EIS system, BIO Logic) for galvanostatic frequency-dependent impedance spectra.

Transfer number of zinc ion (t_{Zn2+}). t_{Zn2+} was measured by Bruce-Vincent method based on potentiostatic polarization at 20 mV in zinc metal symmetric cells. The currents were recorded until it reached steady-states after initial non-steady-state periods. EIS spectra were obtained by changing voltages sinusoidally around 5 V with 1 mV variation from 7 MHz to 0.1 Hz.

Diffusion coefficient (D_{Zn2+}). D_{Zn2+} was calculated by Randles-Sevcik equation describing the scan-rate dependency of voltammetric peak currents. CVs were obtained in a three-electrode configuration: a zinc foil in the presence or absence of αSEI layers as the working electrode; another zinc foil as the counter; and a zinc wire as the reference.

DFT Calculation. All calculations were carried out in the framework of the spin-polarized density functional theory using Vienna ab initio simulation package (VASP) with the projector-augmented wave (PAW) method. We adopt the Hubbard U correction method with the generalized gradient approximation (GGA+U) in the form proposed by Perdew, Burke, and Ernzerhof (PBE) as implemented in VASP. Hubbard parameter U values of 5.0 eV for Zn was used and ferrimagnetic configuration is adopted. The cut-off energy for the plane wave basis set was 500 eV and the ionic positions of all structures were relaxed until the force converged to below 0.01 eV/Å. A Γ-centered k-point meshes of 2×2×2 are adopted.

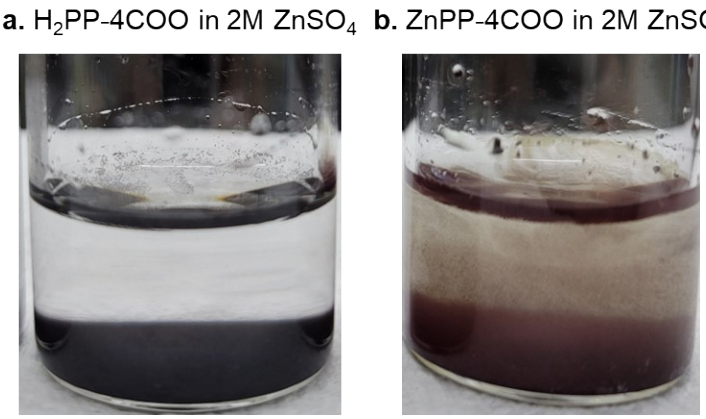

Figure S1. Solubility of PP-4COOs in in 2M $ZnSO_4$. (a) H_2PP-4COO. (b) ZnPP-4COO.

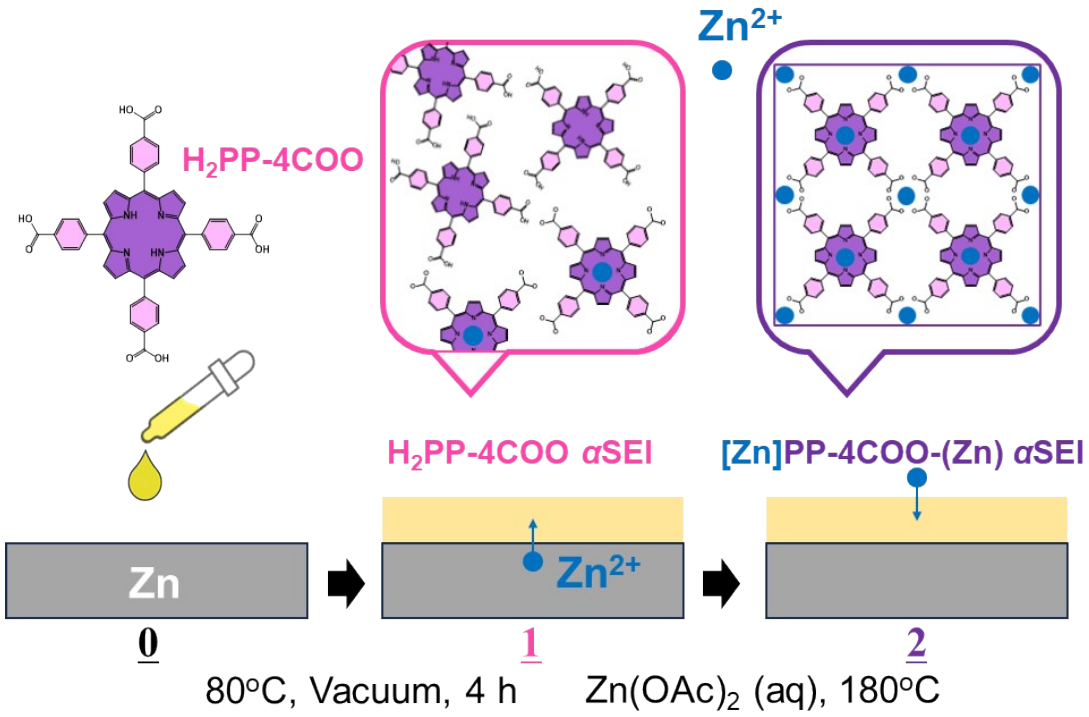

Figure S2. Two-step preparation of the [Zn]PP-4COO-(Zn) αSEI layers on zinc metal foils: [Zn] = Zn^{2+} in the N_4 cages of PP; (Zn) = Zn^{2+} in the O_4 cage between PPs. The H_2PP-4COO αSEI layer (**1**) was prepared in the first step, which was Zn-metalated to form the [Zn]PP-4COO-(Zn) αSEI layers (**2**) in the second step. In the first step, H_2PP-4COO molecules were partially organized via the Zn^{2+}-mediated carboxylate-to-carboxylate linkages of –[COO^-–(Zn^{2+})–^-OOC]$_2$– in the presence of zinc ions originated from zinc metal. In the second step, zinc ions were introduced into the N_4 cages of PP-4COO, and additional carboxylate-to-carboxylate linkages were generated to improve structural ordering of the **2**.

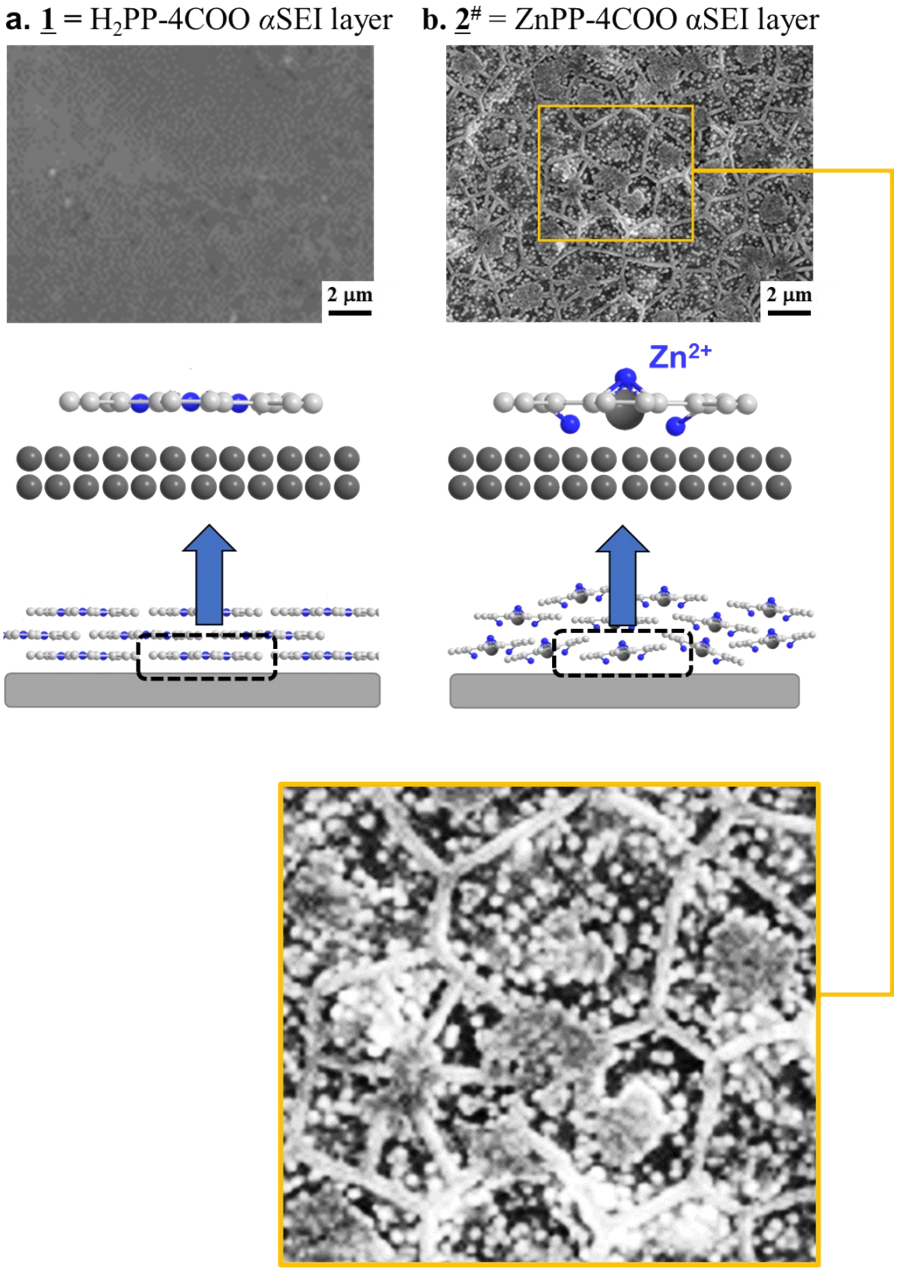

Figure S3. The *α*SEI layers of H_2PP-4COO (1) versus ZnPP-4COO (2#). The ZnPP-4COO *α*SEI layer (**2#**), distinguished from the [Zn]PP-4COO-(Zn) *α*SEI layer (**2**), is the layer prepared from a single step of applying ZnPP-4COO to zinc metal foil (not starting from H_2PP-4COO).

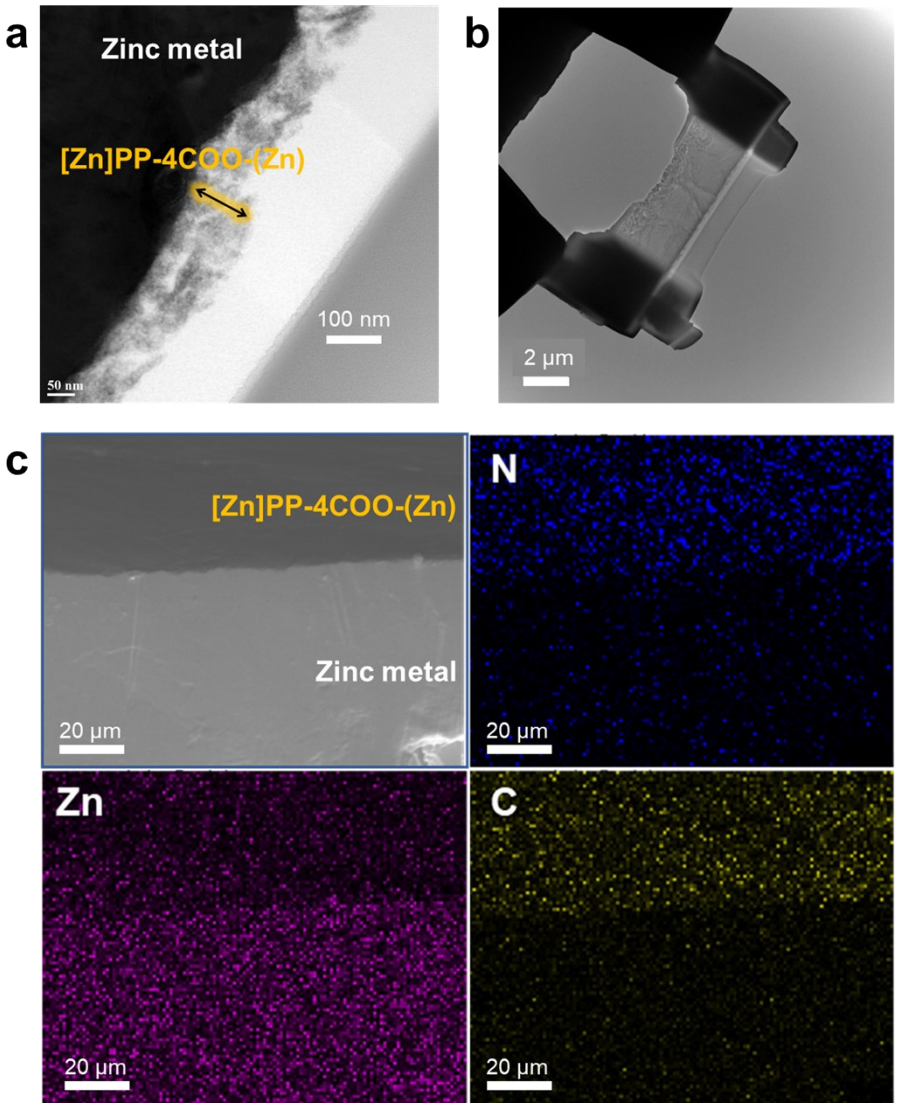

Figure S4. Cross-sectional and surface views of the [Zn]PP-4COO-(Zn) *α*SEI layer (**2**) on zinc metal foil. (**a**) A perpendicular cross-sectional TEM image. The specimens were prepared by focused ion beam (FIB) for TEM. (**b**) A FIB sampling grid for TEM in **a**. (**c**) EDS elemental mappings on the tilted surface of the *α*SEI layer with the zinc metal cross-section. The zinc metal with the αSEI layer on top was immersed in liquid nitrogen and then fractured to prepare the SEM specimen. The specimen was tilted at an angle to allow the *α*SEI layer surface to be visible.

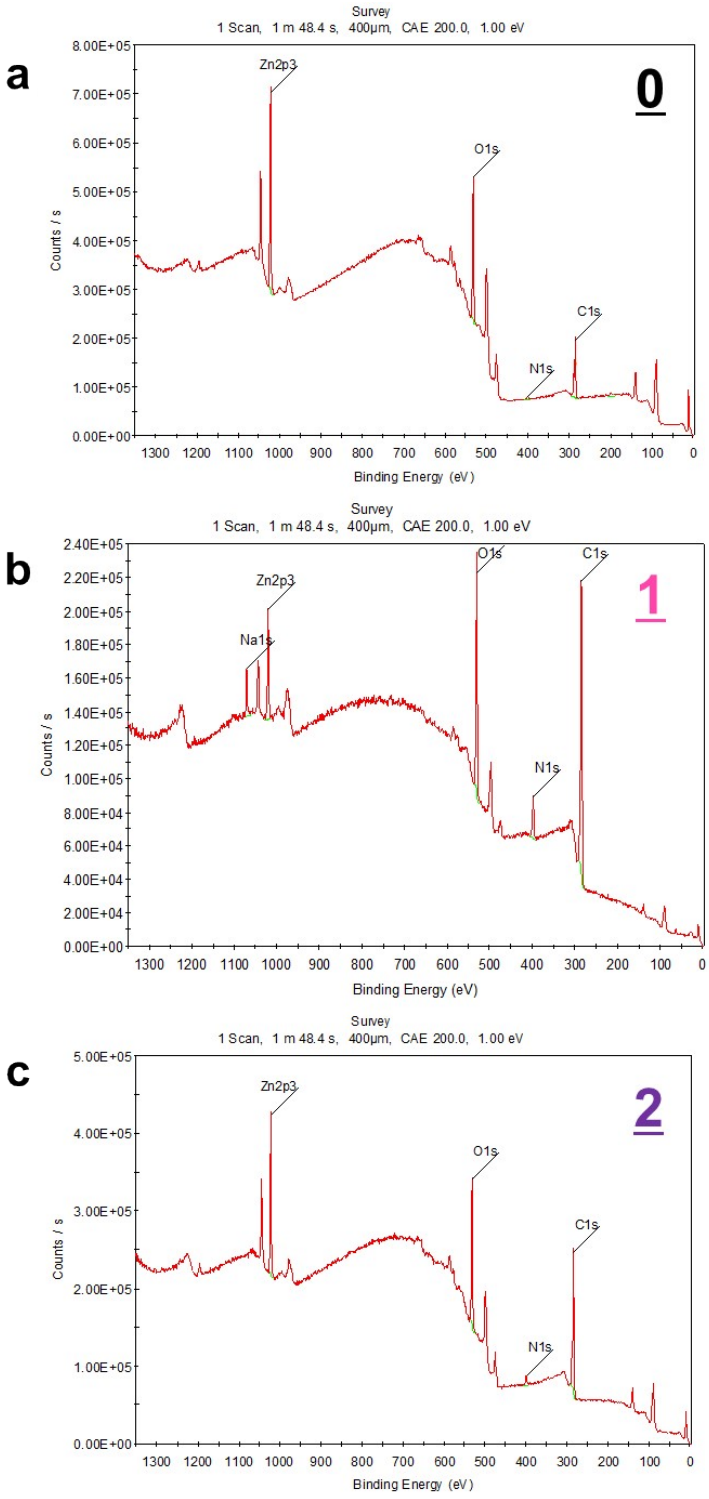

Figure S5. XPS survey spectra of zinc metal with *α*SEI layers on it.

0 = none; **1** = H_2PP-4COO *α*SEI layer; **2** = [Zn]PP-4COO-(Zn) *α*SEI layer.

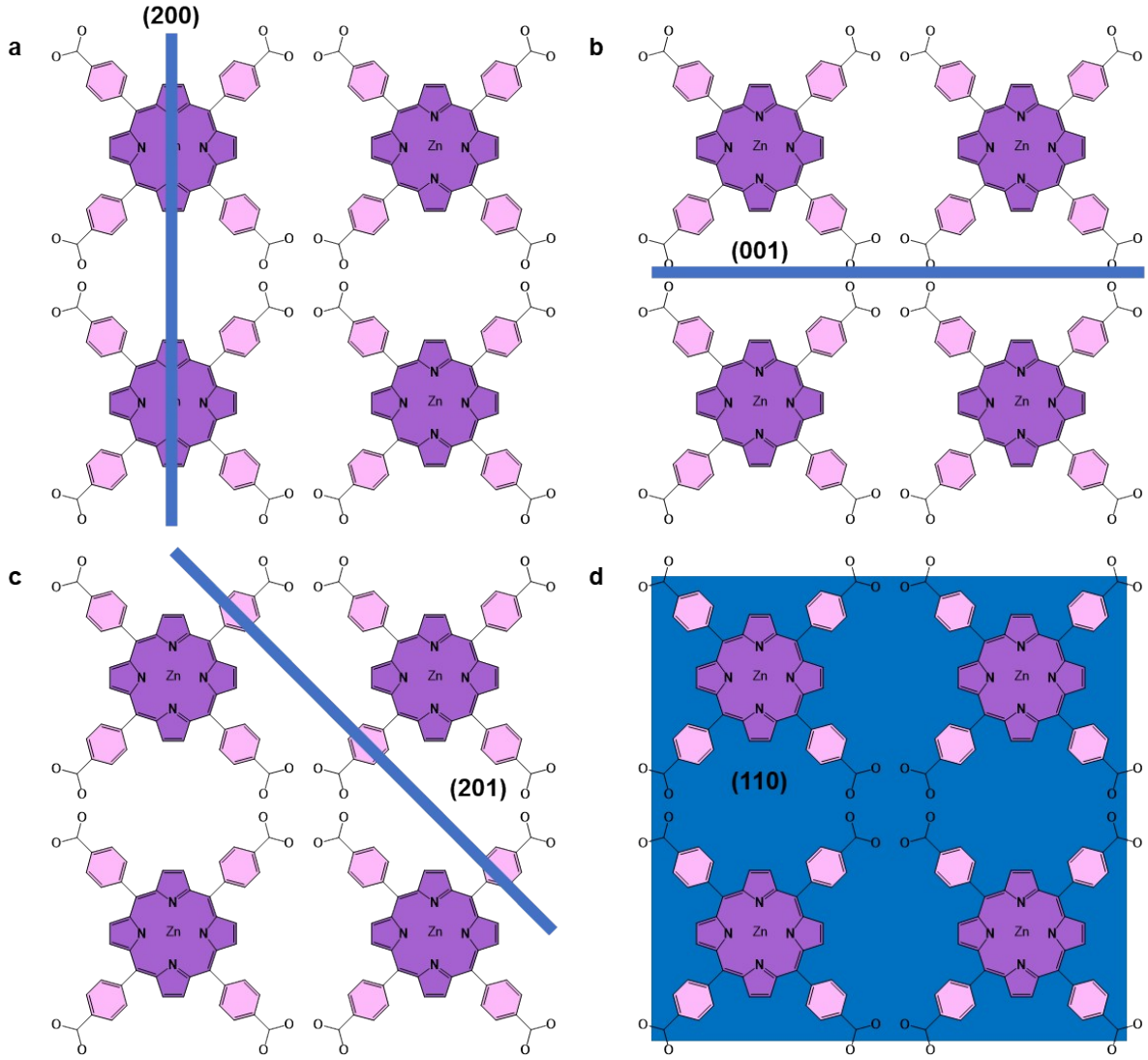

Figure S6. Crystallographic planes of the [Zn]PP-4COO-(Zn) *α*SEI layer (2). (**a**) (200). (**b**) (001). (**c**) (201). (**d**) (110).

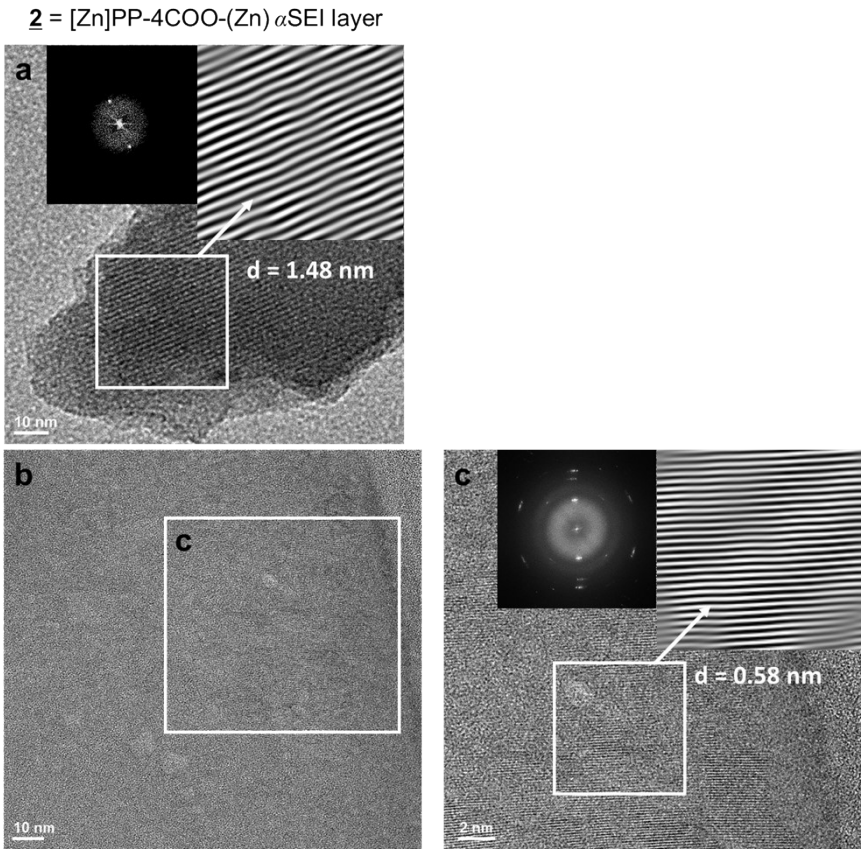

Figure S7. Lattice fringes of the [Zn]PP-4COO-(Zn) αSEI layer (**2**) in TEM images. **Insets in a and c.** FFT patterns on the left and inverse FFT images on the right.

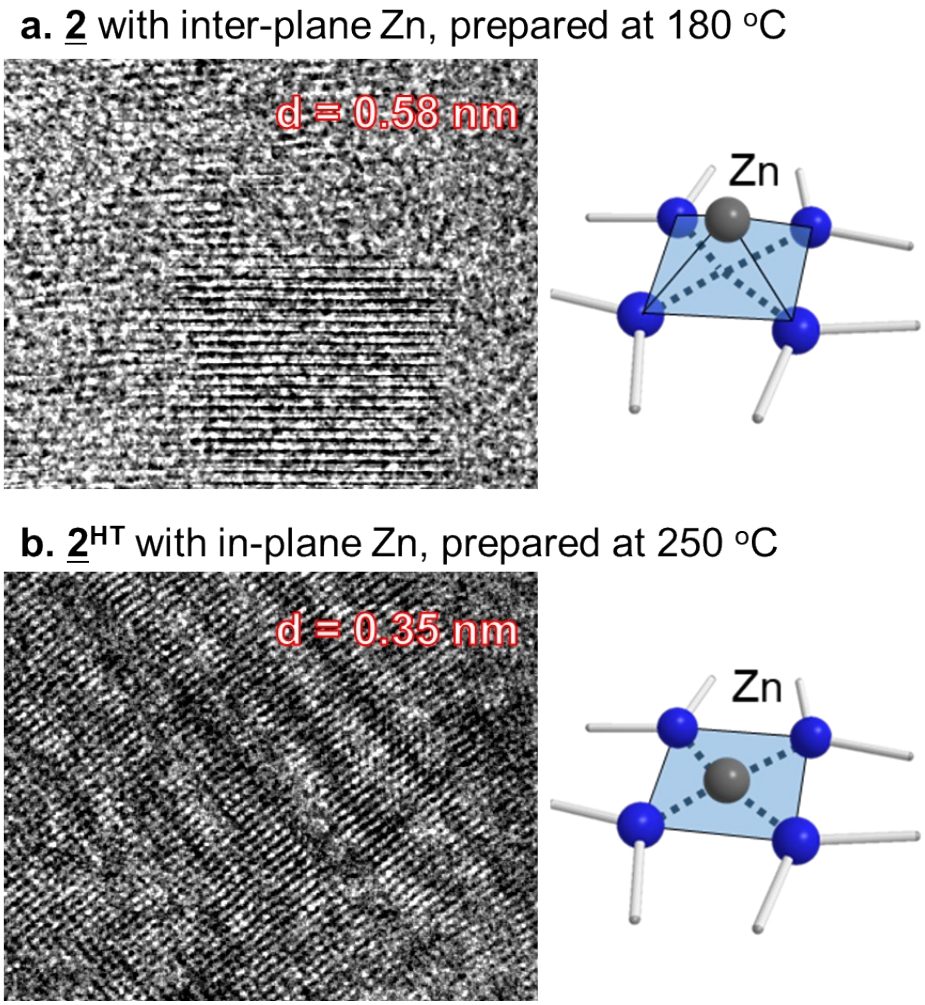

Figure S8. Reduction of d-spacing from **2** to $\mathbf{2}^{HT}$ when the temperature to anneal **1** was changed from 180 °C to 250 °C. The zinc position was changed from the inter-plane N_4 sites (**2**) to the in-plane N_4 sites ($\mathbf{2}^{HT}$). The inter-plane N_4 sites were constructed from two nitrogens from the upper clathrate sheet and two nitrogens from the lower clathrate sheet. On the other hand, all of the nitrogens of the in-plane N_4 sites belonged to a single porphyrinic N_4 cage. (**a** and **b**) TEM images with proposed positions of a zinc ion in a single porphyrinic unit of **2** and $\mathbf{2}^{HT}$, respectively. d-spacings were indicated.

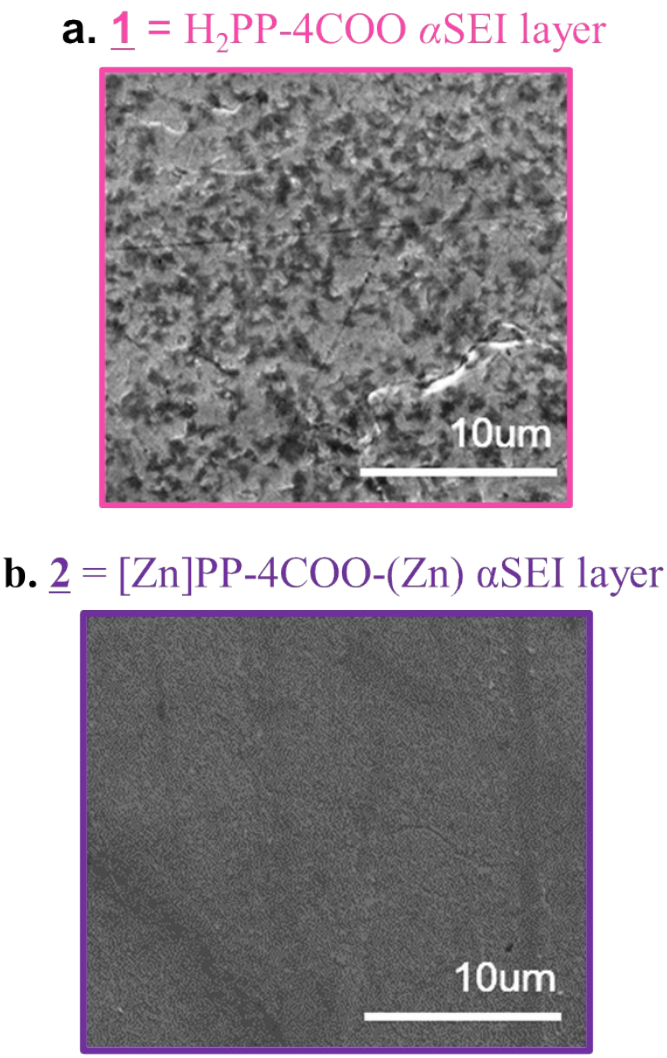

Figure S9. Morphological changes of the electrolyte-side surface of the *α*SEI layers after 10 times repeated zinc metal plating and stripping at 1 mA cm^{-2} in SEM images. (**a**) **1** = H_2PP-4COO *α*SEI layer. (**b**) **2** = [Zn]PP-4COO-(Zn) *α*SEI layer.

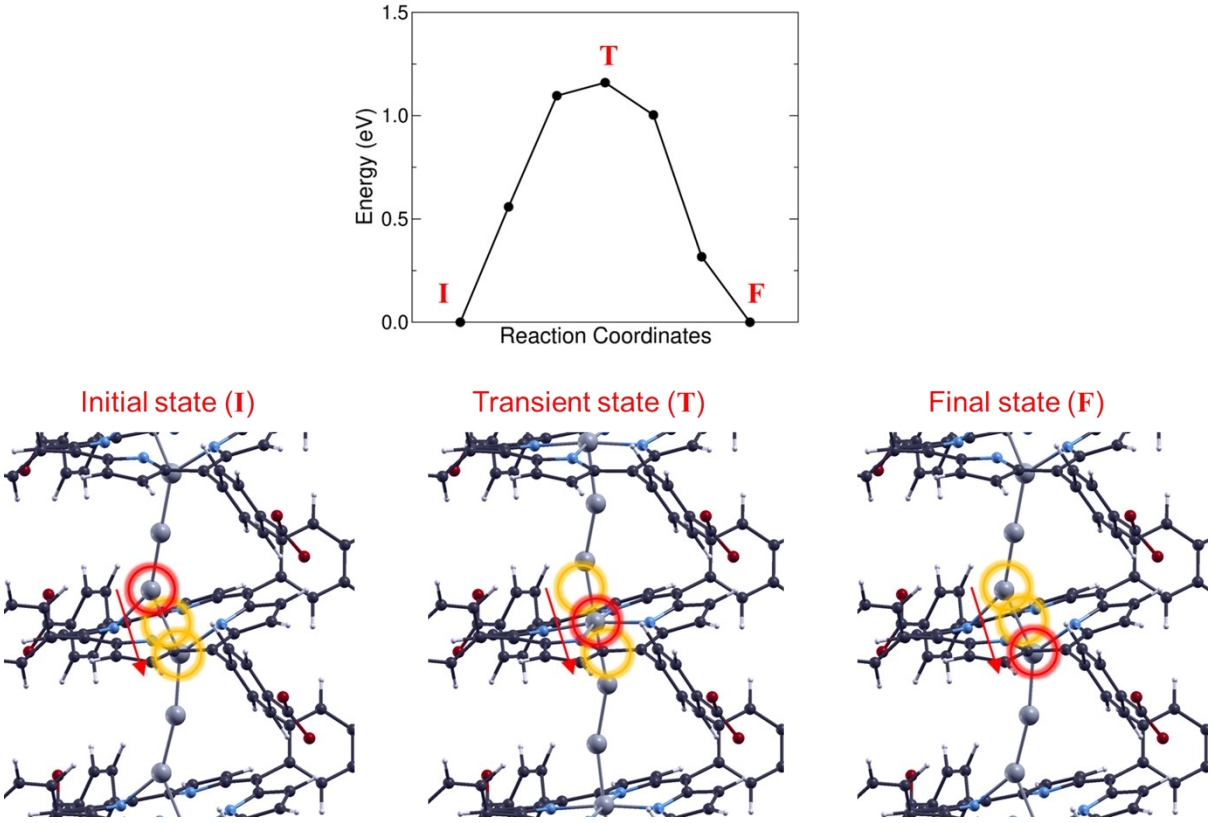

Figure S10. Zn-ion migration barrier along the porphyrinic N_4 channels in Zn^{2+}-rich environments by DFT calculation.

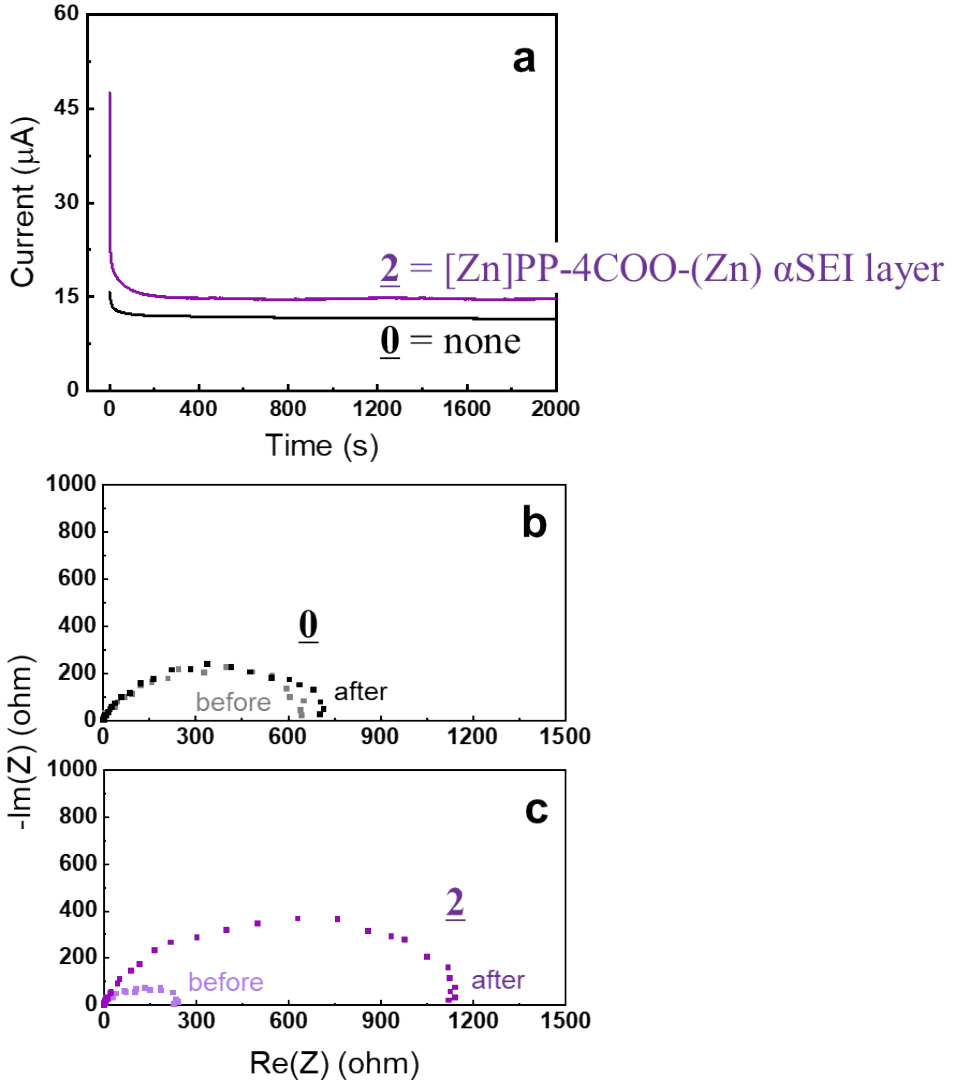

Figure S11. Measuring Zn^{2+} transference number (t_{Zn+}) by Bruce and Vincent method based on potentiostatic polarization: $t_{Zn+} = I_{ss}(\Delta V - I_0R_0)/I_0(\Delta V - I_{SS}R_{SS})$ with ΔV = applied potential for polarization; I = current; R = resistance; subscript 0 = initial values before polarization; subscript SS = steady-state values reached after polarization. Zinc metal symmetric coin cells were employed to investigate the movement of only zinc ions. Zinc ions were steadily supplied from anodes and consumed on cathodes. On the other hand, the zinc metal electrodes were the blocking electrodes for the counter-anions of zinc ions. (**a**) Polarization profiles at 20 mV. The currents reached steady-states after initial non-steady-state periods. (**b** and **c**) EIS spectra in Nyquist plots before and after polarization. Data were obtained by changing voltages sinusoidally around 5 V with 1 mV variation from 100 kHz to 100 mHz.

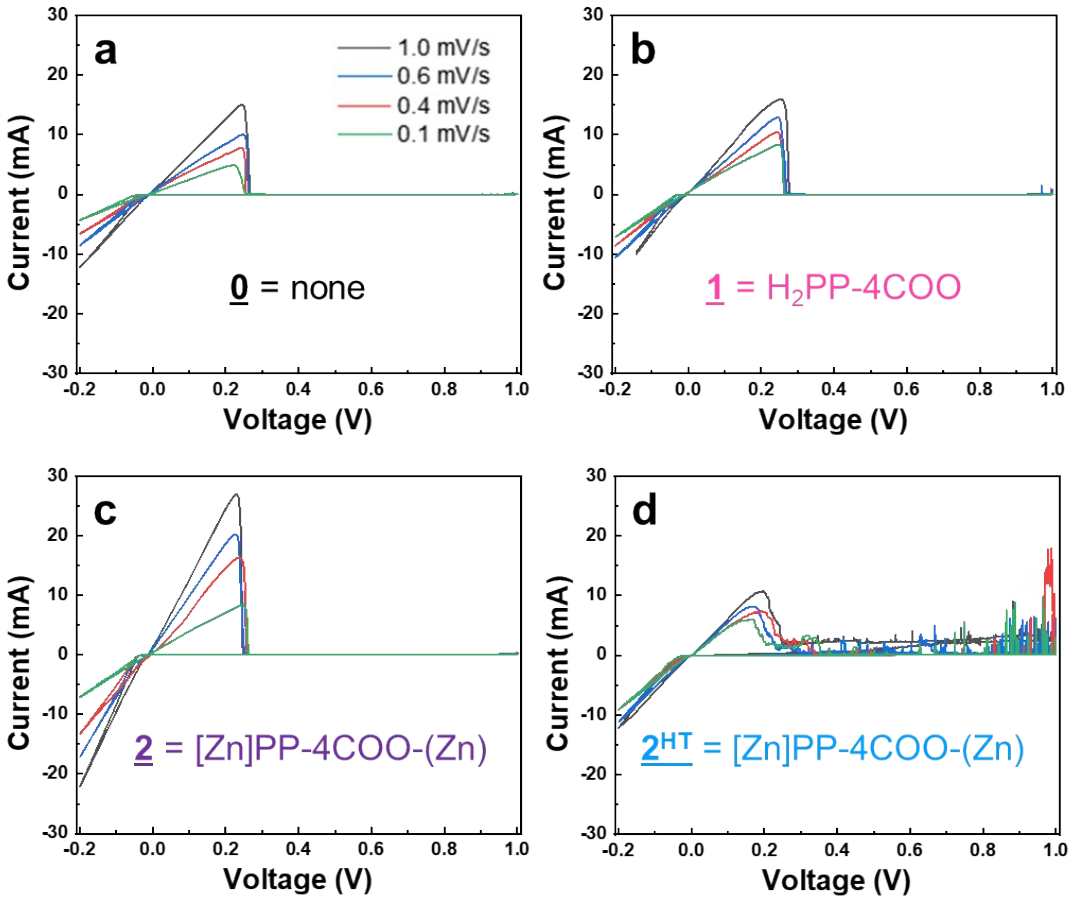

Figure S12. Cyclic voltammograms for calculating zinc ion diffusion coefficient (D_{Zn2+}). Randles-Sevcik equation describing the scan-rate dependency of the voltammetric peak currents was used to calculate the values of D_{Zn2+}. Cyclic voltammograms were measured from a three-electrode system. The anodic peak currents responsible for zinc metal stripping were used for the calculation. (**a**) **0** (*i.e.*, bare zinc metal foil). (**b**) **1**. (**c**) **2**. (**d**) $\mathbf{2}^{\mathbf{HT}}$.

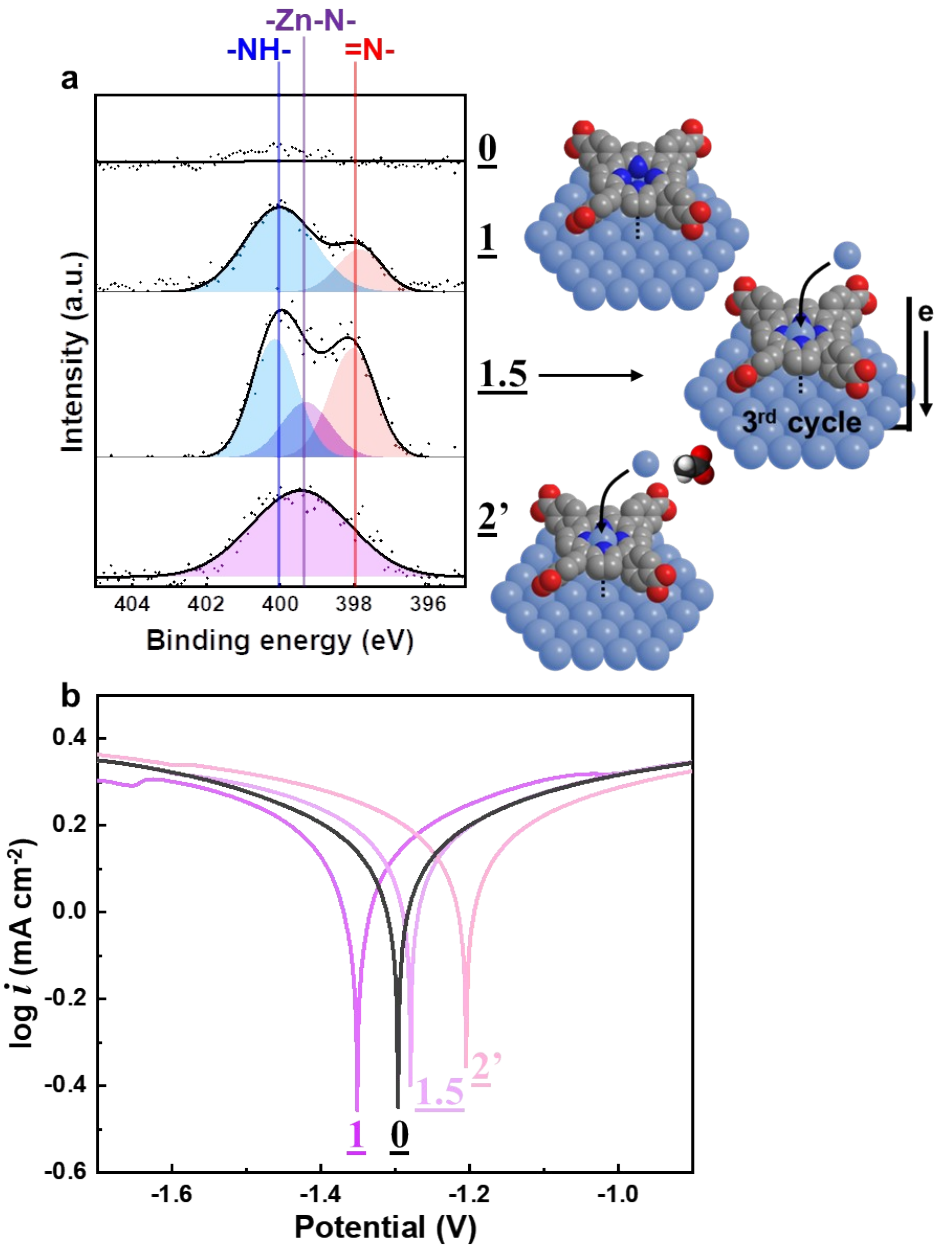

Figure S13. Metalation-dependent corrosion protection of porphyrinic *α*SEI layers: **0** = none; **1** = the H_2PP-4COO *α*SEI layer; **1.5** = partially metalated **1** by an *electrochemical* method (**1.5**); **2**' = fully metalated **1** by a *chemical* method. The **1.5** was prepared by plating zinc metal on **1** in 2 M $ZnSO_4$ (aq) at 0.1 mA cm^{-2} for 10 min. **2'** was prepared by storing **1** in 2 M $ZnSO_4$ for 1 h, taking the sample out of the solution, washing the sample with water, and thermally treating the sample at 180 °C overnight. (**a**) XPS N1s spectra. (**b**) Tafel plots.

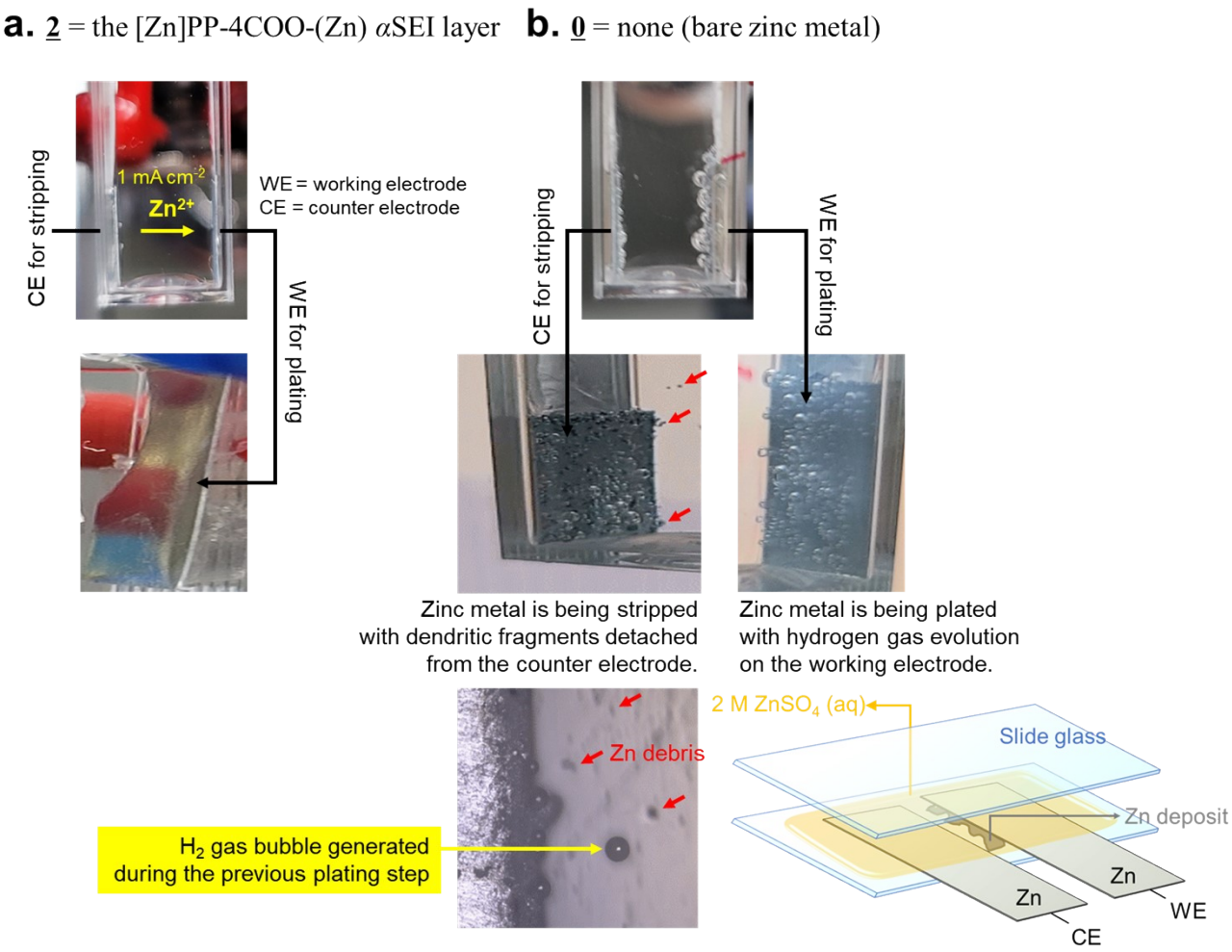

Figure S14. Hydrogen evolution suppression. The still images were captured from video clips (a cuvette cell experiment in **b** from **Supporting Video Clip S1**; a slide glass cell experiment in **b** from **Supporting Video Clip S2**).

(**a**) Zinc metal with the [Zn]PP-4COO-(Zn) αSEI layer on it. (**b**) Bare zinc metal.

Cuvette cells. Zinc symmetric cells with Ag/AgCl as a reference (1 cm distant between 1 cm^2 electrodes) were configured with 2 M $ZnSO_4$ (aq) within transparent cuvettes for visual inspection on metal plating and stripping with hydrogen gas evolution. A constant current at +1 mA cm^{-2} was applied to the working electrode for zinc metal plating for 1 h and then -1 mA cm^{-2} for zinc metal stripping for 1 h. The third plating on the working electrode with the third stripping on the counter electrode was presented.

Slide glass cells. A slide glass cell was used for optical-microscopic inspection. Two zinc metal foils, placed side-by-side, were sandwiched between two slide glasses. 2 M $ZnSO_4$ (aq) was introduced to the gap between the slide glasses. A constant current at +10 mA cm^{-2} was applied to the working electrode for zinc metal plating for 1 h and then -10 mA cm^{-2} for zinc metal stripping for 1 h. The third plating on the working electrode with the third stripping on the counter electrode was presented.

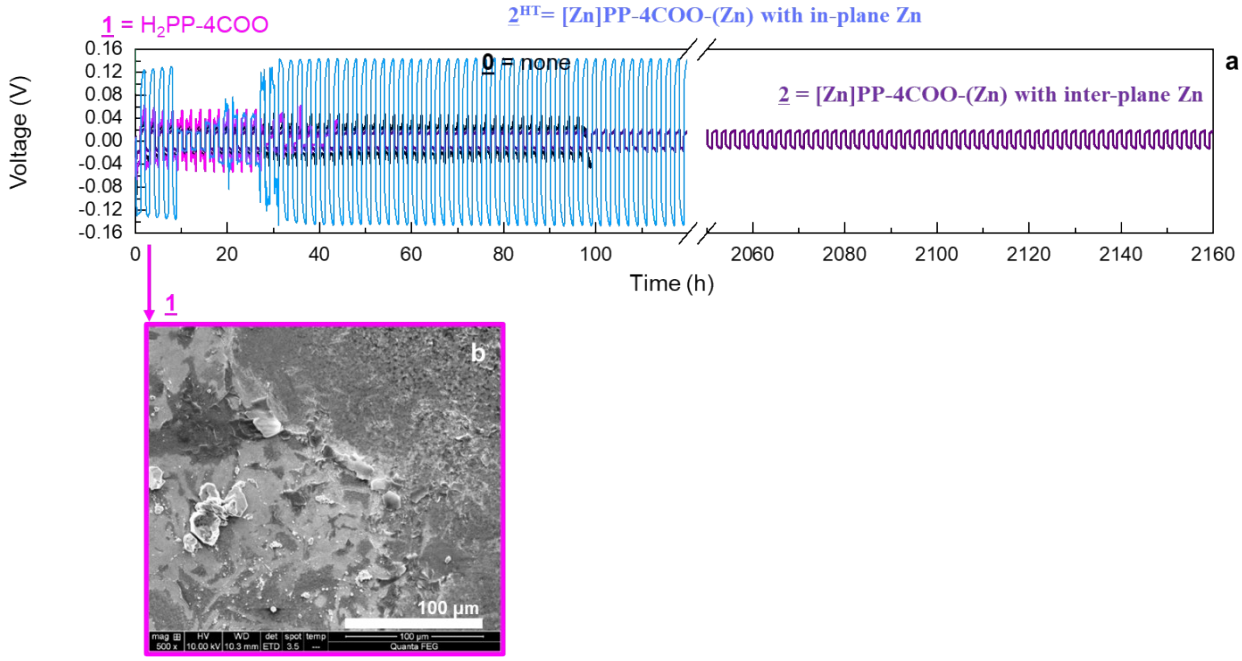

Figure S15. Zinc plating/stripping reversibility in zinc-symmetric cells. 1 mAh cm^{-2} plating/stripping was repeated at 1 mA cm^{-2}. (**a**) **0** versus **1** versus **2** versus $\mathbf{2^{HT}}$. Zinc ions are placed at the inter-plane position for **2** and at the in-plane position for $\mathbf{2^{HT}}$. (**b**) **1** experiencing 10 cycles in a SEM image.

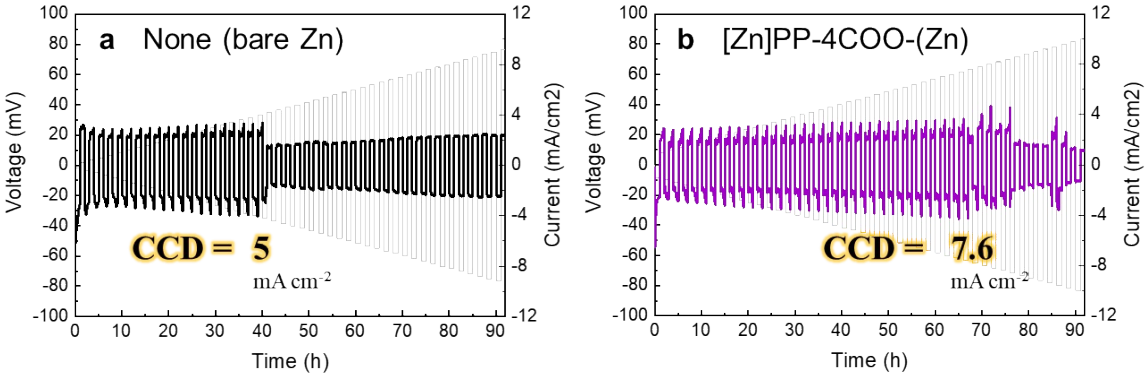

Figure S16. Critical current densities (CCDs). Zinc metal was galvanostatically plated and stripped at increasing current densities, ranging from 1 to 10 mA cm^{-2} in 0.2 mA cm^{-2} increments. Each current density was applied to Zn-Zn symmetric cells for 1 h. (**a**) None (**0**). (**b**) [Zn]PP-4COO-(Zn) (**2**).

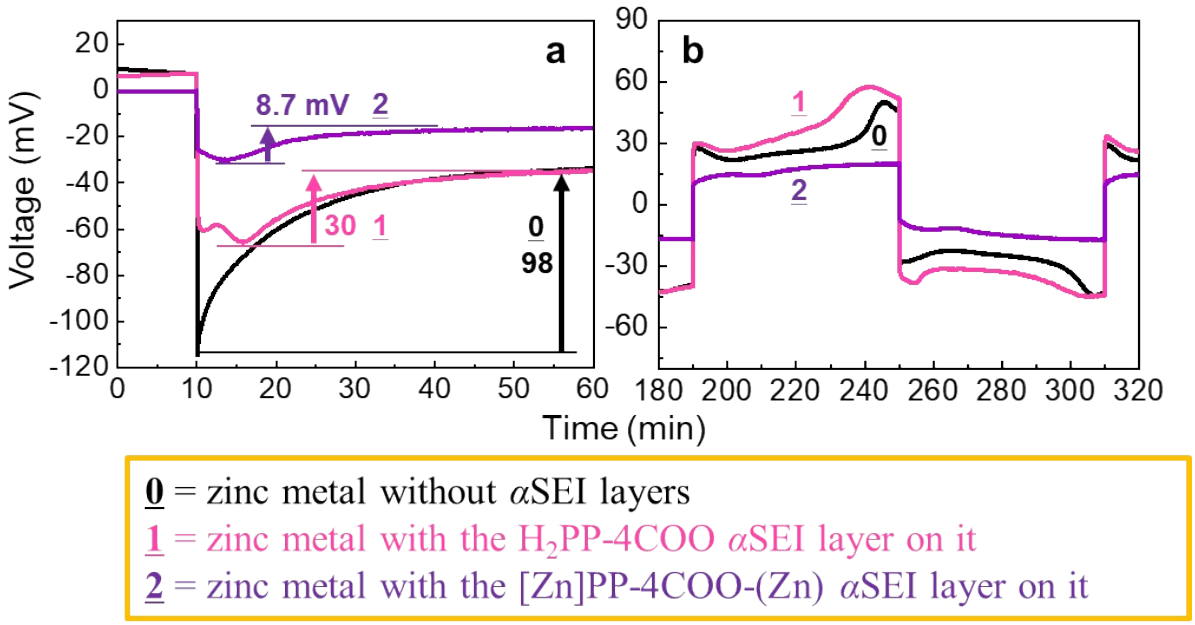

Figure S17. Zinc plating/stripping reversibility. Zinc metal symmetric cells were employed. 1 mAh cm^{-2} zinc metal was repeatedly plated and stripped by 1 mA cm^{-2} (equivalent to 1C). Voltage profiles at the initial period and after 5 h repeated chronopotentiometric operation were presented. SEM images obtained after ten times repeated cycles of plating followed by stripping were presented. (**a** and **b**) Temporal profiles of cell voltage at the 1st plating, and the 2nd stripping followed by the 3rd plating, respectively.

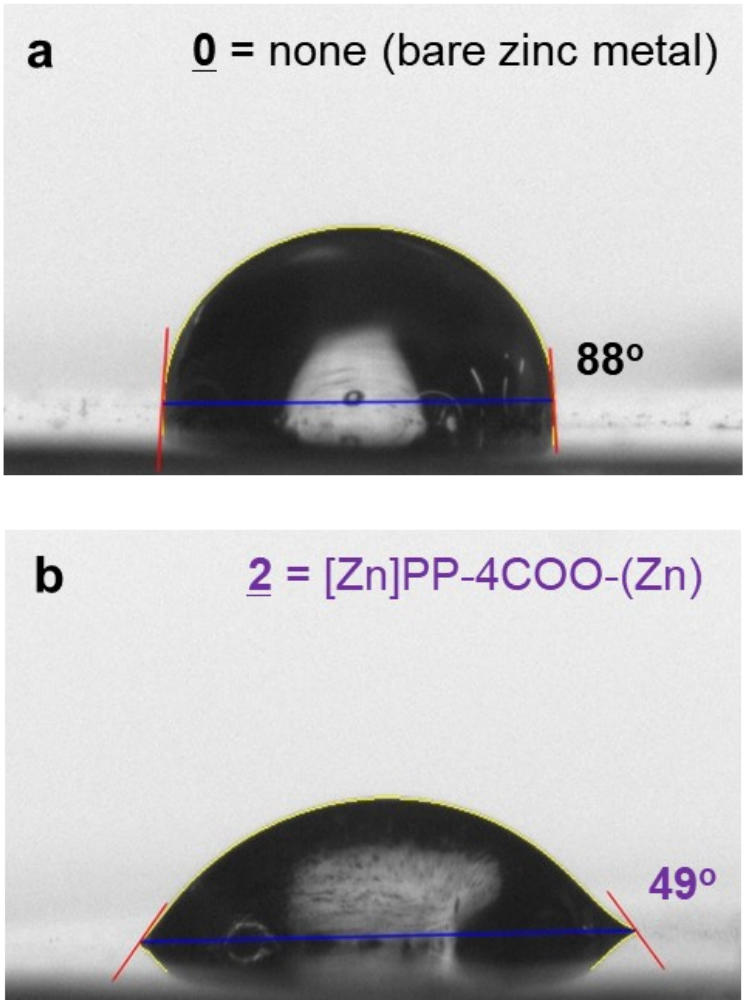

Figure S18. Wettability by contact angle measurement with 2M $ZnSO_4$ (aq). (a) Bare zinc metal. (b) [Zn]PP-4COO-(Zn) αSEI layer.

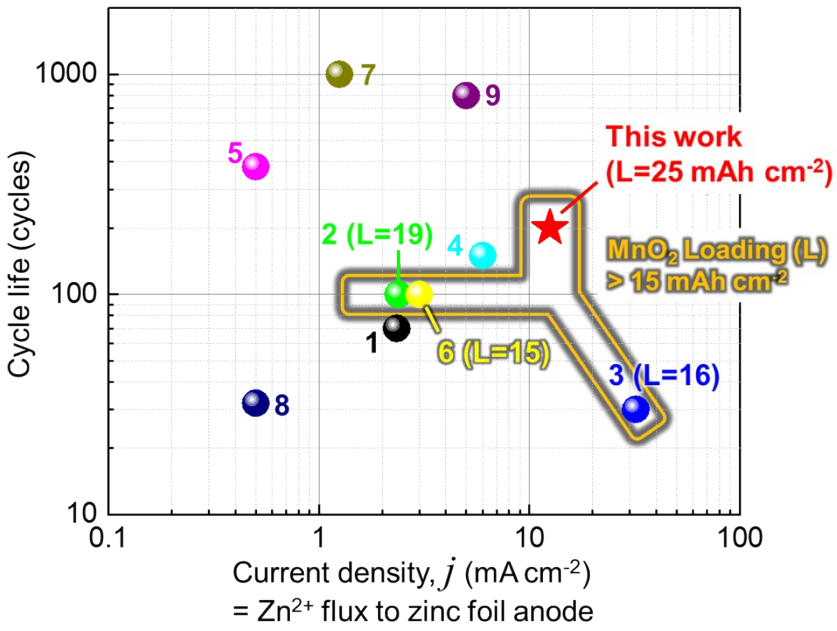

1. R. Wang *et al.*, Adv. Funct. Mater. 2022, **32**, 2207751.
2. J. Dong *et al.*, Energy Storage Mater. 2023, **54**, 875.
3. Y. Meng *et al.*, Chem. Eng. J. 2023, **474**, 145987.
4. S. Zhou *et al.*, Small 2023, **19**, 2303457.
5. J. C. Wu *et al.*, Small 2024, **20**, 2308541.
6. B. Long *et al.*, Adv. Sci. 2022, **9**, 2204087.
7. P. Xue *et al.*, Adv. Funct. Mater. 2021, **31**, 2106417.
8. Y. Pu *et al.*, Chem. Eng. J. 2024, **494**, 153002.
9. Y. Qian *et al.*, J. Energy Chem. 2023, **81**, 623.

Figure S19. Cycle life comparison of MnO_2 ZIB cells. Cycle life = cycle number at which the capacity reaches 75% of the initial capacity. The ZIB cell with 15 mg cm^{-2} MnO_2 cathode and zinc foil anode with the [Zn]PP-4COO-(Zn) αSEI layer (**2**) was compared to high-loading ZIB cells with >15 mg MnO_2 cm^{-2} in previously reported works focusing on engineering zinc anode surface. Reference numbers were indicated. High MnO_2 loading cells (> 15 mAh cm^{-2}) are found within the area surrounded by yellow line. Loading densities were indicated in mAh cm^{-2} for the high-loading cells. Refer to the following **Table S1** for more details.

Table S1. Comparison of MnO_2||Zn ZIB cells. Refer to **Figure S18** for bibliographic information.

Anode	Loading (mg cm^{-2})	Current density (mA cm^{-2})	Current density (A/g)	Cyclability at 75% retention (cycle)	Ref
ZnTe@Zn	3.97	2.34	0.5894	70	1
NH_2-PSiO_x@Zn	**19**	**2.375 (0.5 C)**	**0.125**	**100**	**2**
Zn /expanded graphite	**16**	**32**	**2**	**30**	**3**
$BaTiO_3$@Zn	10	6	0.6	150	4
Zn-In alloy	10	0.5	0.05	380	5
Co-BiOBr@CNT	**15**	**3**	**0.2**	**100**	**6**
hollow SiO_2/TiO2 fiber	1.25	1.25	1	1000	7
W-doped ZnO@Zn	2	0.5	0.25 (1C)	32	8
Sn-BiOCl@CNT	10	5	0.5	800	9
[Zn]PP-4COO-(Zn)	**25**	**12.5**	**0.5**	**200**	**This work**

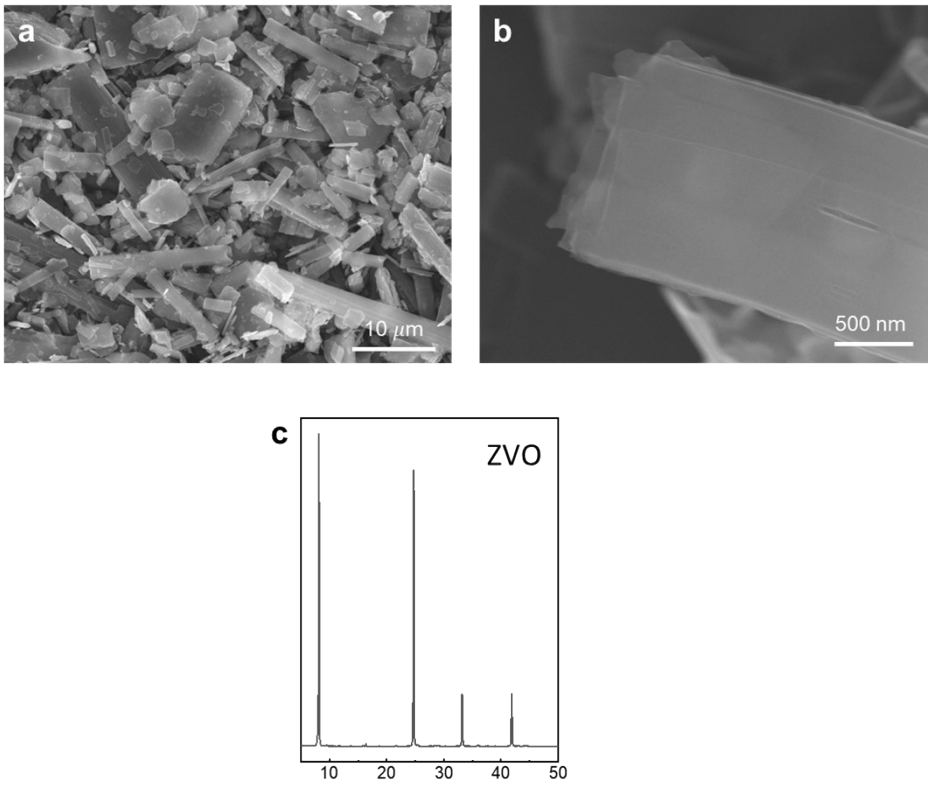

Figure S20. ZVO characterization. (**a** and **b**) SEM images. (**c**) XRD pattern.

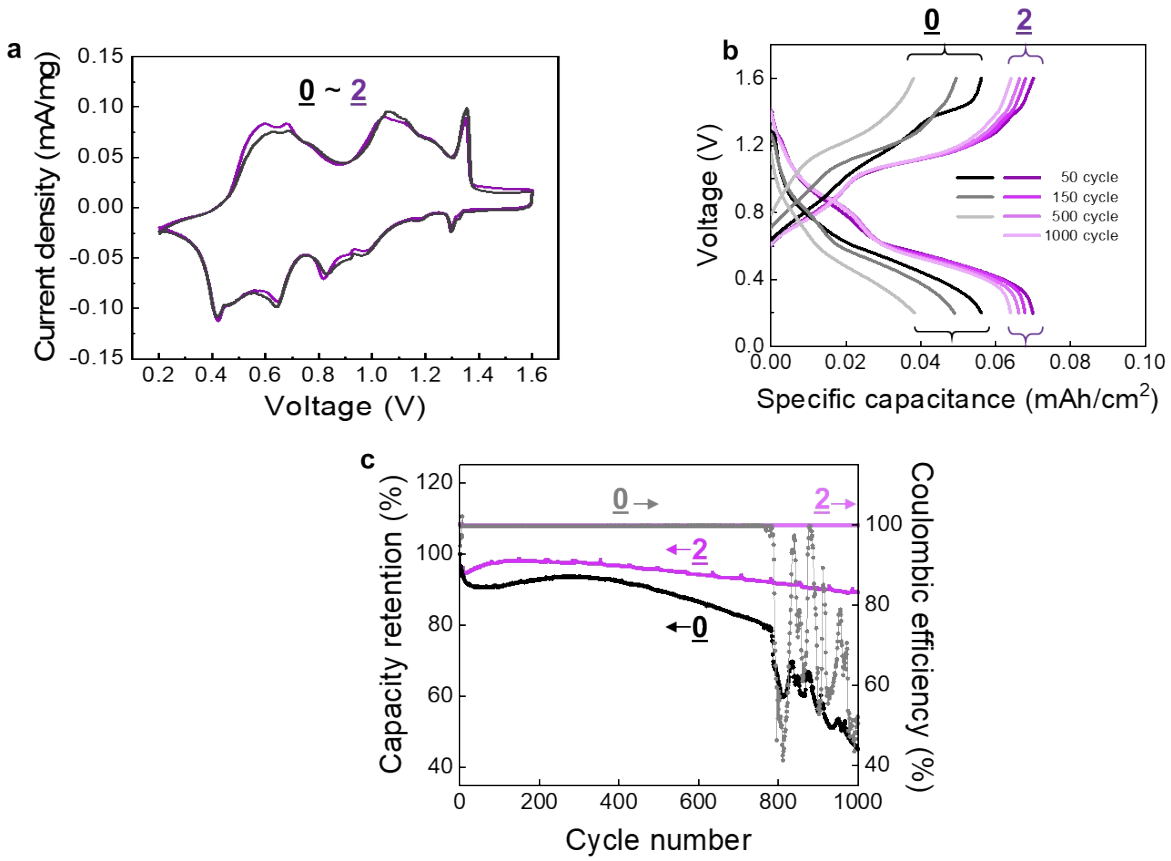

Figure S21. Low-capacity ZVO||Zn ZIB cells with 2 M $ZnSO_4$ (aq) for investigating the effect of the *α*SEI layer 2 on HER suppression. To realize the HER-dominant situation with relatively less significant plating problems, ZVO||Zn cells having a low-capacity cathode at 70 μAh cm^{-2} were designed to be operated at low Zn^{2+} flux (1000 mA g^{-1} x 1.4 mg cm^{-2} = 1.4 mA cm^{-2}) of a significantly short duration (3 min). Both Zn^{2+} flux and duration time for the ZVO||Zn cells were a tenth of those for the MnO2||Zn cell presented above: ZVO versus MnO_2 = 1.4 versus 12.5 mA cm^{-2}; 3 min versus 30 min; 70 versus 3000 μAh cm^{-2} for their cathode capacity. (**a**) CVs at 0.1 mV s^{-1}. The cathode was connected to a potentiostat as the working electrode. Two different anodes were compared with the cathode fixed. (**b**) Voltage profiles. (**c**) Retention of capacity and coulombic efficiency along repeated charge/discharge at 1000 mA g^{-1} based on cathode active material mass.

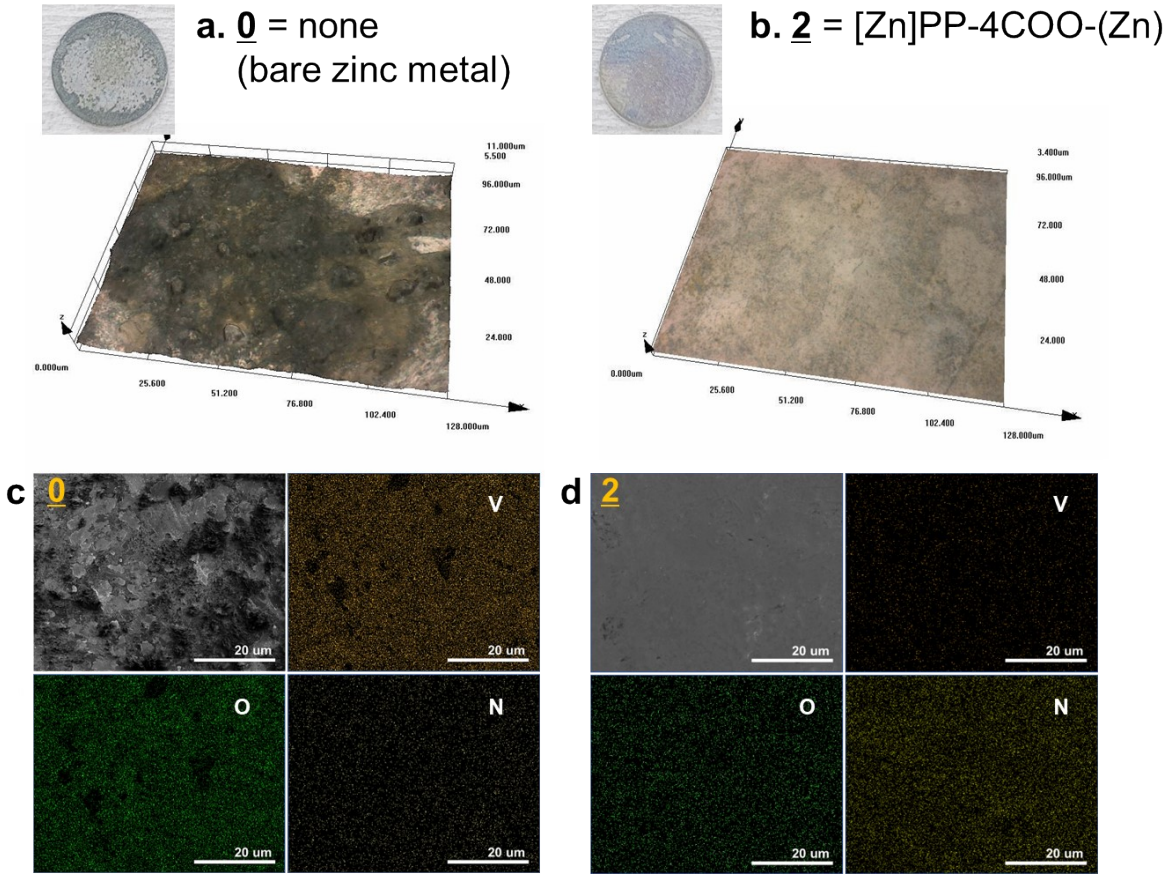

Figure S22. Zinc metal anodes in ZVO||Zn cells after 10 times repeated charging/ discharging cycles. (**a** and **b**) Confocal-microscopic images of the surface of bare zinc metal (**0**) and zinc metal with the [Zn]PP-4COO-(Zn) αSEI layer on it (**2**), respectively. (**c** and **d**) SEM images with EDS elemental mappings of **0** and **2**, respectively.